

# Origin and structure of transonic buffet on airfoils

J.D. Crouch<sup>1</sup>, A. Garbaruk<sup>2</sup>,  
D. Magidov<sup>2</sup> AND A. Travin<sup>2</sup>

<sup>1</sup>The Boeing Company, Seattle, WA 98124-2207, USA

<sup>2</sup>Saint-Petersburg Polytechnic University, St. Petersburg, Russia

Buffeting flow on transonic airfoils serves as a model problem for the more complex three-dimensional flows responsible for airplane-buffet phenomena. The origins of transonic airfoil buffet are linked to a global instability, which leads to shock oscillations and dramatic lift fluctuations. The problem is analyzed using the Reynolds-averaged Navier-Stokes equations, which are necessary to cover the high Reynolds numbers where transonic buffet occurs. Results from global-stability analysis are shown to be in good agreement with experiments and numerical simulations. The unstable modes provide insight into the basic character of buffeting flow at near-critical conditions.

---

## 1. Introduction

Transonic buffet is characterized by large-scale lift oscillations that can limit the flight envelope of aircraft. This generally occurs at the higher lift coefficients associated with higher-altitude flight. Many of the features observed in airplane buffet are also observed in the unsteady flow fields of transonic airfoils. Starting at a moderate lift coefficient, as the angle of attack is increased the shock intensifies and moves aft over the airfoil. At sufficiently-high angles of attack, the boundary layer separates – either as a bubble at the foot of the shock, or at the trailing edge. Further increases in the angle of attack often lead to separation at the shock extending to the trailing edge. At some point in this process, the flow can become highly unsteady with large oscillations in the shock position leading to large lift fluctuations.

The practical problem of airplane buffet results from a structural response to the buffeting flow field. Predictions of airplane buffet are often highly empirical, attempting to link different features of the flow field with measured accelerations of the airplane structure. Meanwhile, the prediction of the onset and character of the unsteady flow field is of itself a great challenge. The transonic airfoil has been used as a model problem for understanding the unsteady forcing since it exhibits features similar to the airplane buffeting response. Controlled experiments show a fairly-sudden onset of flow unsteadiness as the angle of attack is increased (McDevitt & Okuno 1985; Jacquin *et al.* 2005). This is characterized by large pressure fluctuations near, and downstream of, the shock.

A number of empirical criteria have been proposed for predicting the onset of buffeting flow; see, for example, the review of Lee (2001). These are linked to heuristic models, which describe the structure of the buffeting flow field. One of the simplest of these criteria is based only on a threshold for the pre-shock Mach number. Other models consider zones of separation, and how these vary with changes in the shock strength or position. While some of these models provide useful descriptors for the flow behaviour, they have not been effective as predictors for the buffet onset. Lee (2001) notes in his review that even though the buffet problem has been known for fifty years, the physical mechanism for buffet onset is still not fully understood.

Meanwhile, the origins of airfoil-buffet onset have been linked to a global instability of the underlying flow field (Crouch, Garbaruk & Magidov 2007). The stability theory has been shown to effectively predict the buffet boundary for two different airfoils (Crouch, Garbaruk & Magidov 2007; Crouch, Garbaruk, Magidov & Jacquin 2007), and has also been shown to predict the structure of the buffeting velocity field (Crouch, Garbaruk, Magidov & Jacquin 2007). Here we make use of a combination of global-stability theory and unsteady Reynolds-averaged Navier-Stokes (URANS) simulations to study the origin and structure of the buffeting flow, and to assess empirical and mechanistic descriptors for buffet onset.

## 2. Global-stability theory

Global-stability theory has been used to analyze a wide variety of low-speed laminar flows, as reviewed by Theofilis (2003). Here we follow the formulation of Crouch, Garbaruk & Magidov (2007), which accounts for high Reynolds numbers and compressible flow. We consider two-dimensional transonic flow, with Reynolds numbers of  $Re_C = O(10^7)$ . At these Reynolds numbers, much of the viscous shear-layer flow is turbulent. However, in the current study we are interested in time scales much longer than the characteristic eddy time scales. Thus, we employ the Unsteady Reynolds Averaged Navier-Stokes equations (URANS), where the large-scale unsteadiness is explicit, but the effects of the turbulence fluctuations are modeled to provide closure for the averaged Reynolds stresses. The turbulence model used is the compressible form of the Spalart-Allmaras model (Spalart & Allmaras 1994) – including the compressibility correction (Spalart 2000). Here, we focus on flows that can be treated as either laminar or “fully turbulent,” which removes the need for the trip-term functions. This leads to a set of five equations: continuity, streamwise momentum, transverse momentum, energy, and a modified eddy-viscosity equation. These equations can be written in terms of the primitive variables,  $q = \{\rho, u, v, T, \tilde{\nu}\}$  as follows:

$$\frac{\partial}{\partial t} M[q] + Q[q] + N[q, q] = 0, \quad (1)$$

where  $M$  and  $Q$  are linear operators and  $N$  contains all nonlinear terms.

The boundary conditions imposed on the surface of the body are:

$$\begin{aligned} u = v = 0, \\ \frac{\partial \rho}{\partial n} = \frac{\partial T}{\partial n} = 0, \\ \tilde{\nu} = 0, \end{aligned} \quad (2)$$

where  $\partial/\partial n$  is a derivative normal to the surface and the density condition is derived from the equation of state. The far-field conditions used in the compressible computations involve not only the primary variables  $\rho, u, v, T, \tilde{\nu}$  but also the Riemann invariants. These conditions, expressed in terms of the primary variables, are given as:

$$\begin{aligned} I_1 &= V_n + \frac{2a}{(\gamma - 1)} = k_x u + k_y v + \frac{2}{(\gamma - 1)} \sqrt{\gamma RT}, \\ I_2 &= V_n - \frac{2a}{(\gamma - 1)} = k_x u + k_y v - \frac{2}{(\gamma - 1)} \sqrt{\gamma RT}, \\ I_3 &= V_\tau = k_y u - k_x v, \\ I_4 &= \frac{RT}{\rho^{\gamma-1}}. \end{aligned} \quad (3)$$

Here  $k_x, k_y$  are the local directional cosines of the boundary normal. These conditions are imposed on the subsonic boundaries in the following way. On the inlet boundary,  $\tilde{\nu}$  and invariants  $I_1, I_3, I_4$  are given and  $I_2$  is extrapolated from the computational domain. On the outlet boundary,  $\tilde{\nu}$  and  $I_1, I_3, I_4$  are extrapolated from the computational domain and  $I_2$  is given.

The state vector describing the total flow field can be decomposed into a steady state  $\bar{q} = \{\bar{\rho}, \bar{u}, \bar{v}, \bar{T}, \bar{\tilde{\nu}}\}$  and an unsteady vector  $q' = \{\rho', u', v', T', \tilde{\nu}'\}$ ,  $q = \bar{q} + q'$ . The vector  $\bar{q}$  is a solution to the steady form of equations (1)-(3) – that is with  $\partial\bar{q}/\partial t \equiv 0$ . The steady-state RANS equations are normally re-written in conservative form before solving them numerically. For conditions close to steady state, the unsteady component  $q'$  can be considered a small perturbation to the vector  $\bar{q}$ . Substituting  $q = \bar{q} + q'$  into equation (1), canceling the terms governing  $\bar{q}$ , and linearizing the equations in terms of  $q'$  yields:

$$\frac{\partial}{\partial t} M[q'] + N_{\bar{q}}[q'] = 0. \quad (4)$$

The linear operator  $M$  contains the terms associated with the time derivatives from the original equation (1). The linear operator  $N_{\bar{q}}$  consists of linear terms from the original equations, and the terms generated by nonlinear interactions between  $\bar{q}$  and  $q'$ .

The unsteady perturbation to the steady-state flow  $\bar{q}(x, y)$  can be represented by time-harmonic modes of the form

$$q'(x, y, t) = \hat{q}(x, y) \cdot \exp(-i\omega t). \quad (5)$$

The function  $\hat{q}$  describes the mode shape, and  $\omega$  is the frequency. In general, both  $\hat{q}$  and  $\omega$  can be complex, so the physical solution is taken as the real part of equation (5). Substituting (5) into (4) and rescaling the terms yields a system of equations for  $\hat{q}$  and  $\omega$ :

$$-i\omega\hat{q} + L(\bar{q}) \cdot \hat{q} = 0, \quad (6)$$

with  $L$  being a second-order differential operator.

The boundary and far-field conditions are obtained by introducing  $q = \bar{q} + q'$  into the expressions (2) and (3), canceling the terms governing the steady state, and linearizing with respect to  $q'$ . Then substituting (5) for  $q'$  yields the boundary conditions for  $\hat{q}$ :

$$\begin{aligned} \hat{u} = \hat{v} &= 0, \\ \frac{\partial \hat{\rho}}{\partial n} = \frac{\partial \hat{T}}{\partial n} &= 0, \\ \hat{\nu} &= 0. \end{aligned} \quad (7)$$

The far-field conditions for the inlet boundary are given by:

$$\begin{aligned} \hat{I}_1 = \hat{I}_3 = \hat{I}_4 = \hat{\nu} &= 0, \\ \frac{\partial \hat{I}_2}{\partial n} &= 0, \end{aligned} \quad (8)$$

and for the outlet boundary:

$$\begin{aligned} \frac{\partial \hat{I}_1}{\partial n} = \frac{\partial \hat{I}_3}{\partial n} = \frac{\partial \hat{I}_4}{\partial n} = \frac{\partial \hat{\nu}}{\partial n} &= 0, \\ \hat{I}_2 &= 0. \end{aligned} \quad (9)$$

The variables  $\hat{I}_1$ ,  $\hat{I}_2$ ,  $\hat{I}_3$ , and  $\hat{I}_4$  are the linearized versions of the Riemann invariants, eqn. (3). Additional details are given in Crouch, Garbaruk & Magidov (2007). Equations (6)-(9) describe an eigenvalue problem governing the complex frequency  $\omega$  and mode shape  $\hat{q}$ .

Both the steady flow and the eigenvalue problem are solved numerically using finite differencing. The steady flow is calculated using the NTS code (Strelets 2001), which is based on an implicit finite-volume formulation on a structured multi-block overlapping grid. A third-order Roe scheme is used for the inviscid fluxes Roe (1981), and a second-order central difference scheme is used for the viscous momentum and heat fluxes. The convective terms in the turbulence-model equation are approximated using a first-order upwind scheme. For unsteady calculations, the time derivatives are approximated with second-order backward differences (three-layer scheme) with sub-iterations (Strelets 2001).

In order to reduce the numerical dissipation of the upwind differencing, we use a ‘‘hybrid’’ scheme for the stability equations (Crouch, Garbaruk & Magidov 2007). This is weighted between upwind and central differencing:

$$\Delta_H = \alpha_H \Delta_{3u} + (1 - \alpha_H) \Delta_{4c}, \quad 0 \leq \alpha_H \leq 1. \quad (10)$$

The finite difference operators  $\Delta_{3u}$  and  $\Delta_{4c}$  correspond to the third-order upwind and fourth-order centered schemes respectively and  $\alpha_H$  is the weighting constant. The influence of the weighting constant is considered in Crouch, Garbaruk & Magidov (2007); the current results are based on  $\alpha_H = 0.2$ . For the stability equations, the upwind finite-differencing approximations are linear.

The steady base flow and the stability equations are solved on the same grid. The discretized eigenvalue problem results in a matrix of dimension  $O(100,000)$ , which is solved using the implicitly restarted Arnoldi method (Lehoucq *et al.* 1998). Prior to solution, a spectral transformation is used to transform the eigenvalues in the neighborhood of  $\omega^*$  into extreme values for the system. This is achieved using the ARPACK routines (Lehoucq *et al.* 1998) with the shift-invert mode. The value of the prescribed frequency  $\omega_r^*$  is chosen based on experimental data, where available, or based on the basic model scaling. The prescribed growth rate  $\omega_i^*$  is taken to be positive. By varying the prescribed frequency, a search can be made for all unstable modes over a given range. Instability, signifying the onset of unsteadiness, occurs when  $\omega_i > 0$ .

An unsteady perturbation to a flow field containing a shock will have a large response at the shock location. As a shock is better resolved it becomes thinner, and the unsteady response takes the form of a delta function. A typical steady-flow solution captures the shock over two or three grid points. A linear perturbation to this flow field will exhibit ‘‘ringing’’ in the neighborhood of the shock unless

some form of shock smoothing is done. The ringing due to the shock will contaminate the eigenfunction, and may alter the eigenvalue. To address this, we perform a two-step shock smoothing after the steady flow is calculated. First, the original solution to the steady RANS equations is smoothed over the entire computational domain, resulting in a smoothed field  $\bar{q}_{smooth}$ . The smoothing is performed in the dominant flow direction over  $N_{SC}$  smoothing cycles. During each cycle, the flow variables are modified according to:

$$\bar{q}(i, j) = \bar{q}(i, j) + 0.5 c_i [\bar{q}(i + 1, j) - 2\bar{q}(i, j) + \bar{q}(i - 1, j)], \quad (11)$$

where  $c_i$  is a smoothing coefficient that controls the amount of smoothing per cycle. The field  $\bar{q}_{smooth}$  is defined by the value of  $\bar{q}$  after  $N_{SC}$  smoothing cycles. For all of the results presented in this paper,  $c_i = 0.1$ . In the second step, the smoothed field is blended with the original field in the neighborhood of the shock, where the grid spacing is very fine; away from the shock,  $\bar{q}$  is given by the original field.

### 3. Buffet onset

To examine the origins of buffet, we focus on the NACA0012 airfoil as considered in the experiments of McDevitt & Okuno (1985). The experiments show an onset of buffeting flow as the angle of attack is increased at a fixed Mach number. Subsequently, the level of unsteadiness, as measured by surface pressure, increases with the angle of attack. Figure 1 shows Mach contours from RANS calculations at angles of attack just below the buffet onset for the different Mach numbers. The three images are qualitatively similar, showing a relatively strong shock followed by a dramatically-thickened boundary layer. The Mach numbers just before the shock are  $M_1 = 1.42, 1.40$  and  $1.38$  for the free-stream Mach numbers  $M = 0.72, 0.76$  and  $0.80$ , respectively. The value  $M_1$  does not provide an obvious indicator for the buffet onset, although the general levels fall between the  $M_1 = 1.34$  (observed on the bi-convex airfoil (Mabey, Welsh & Cripps 1981)) and  $M_1 \approx 1.42 - 1.52$  (observed on a more conventional wing airfoil (Lee 1990)).

Following the global-stability analysis, the origin of unsteadiness is predicted by the onset of instability. Figure 2 shows the variation of the instability growth rate as a function of angle of attack for  $M = 0.76$ . The different curves signify different levels of shock smoothing prior to the stability calculation, with  $N_{SC} = 0$  corresponding to no smoothing. The buffet onset is predicted to occur at  $\alpha \approx 3.02^\circ$  (with  $N_{SC} = 80$ ). The smoothing has been shown to affect the growth rate due to the change in the shock thickness (Crouch, Garbaruk & Magidov 2007). Thus, the streamwise grid spacing around the shock also has an influence on the growth rate. For the grid spacing of Figure 2 ( $\Delta x_s/c = 0.0015$ ), the smoothing (with  $N_{SC} = 80$ ) results in a shift of  $\alpha = 0.03$  in the buffet onset, as compared to no smoothing. This is considered to be a small source of uncertainty compared to other potential sources, such as nonlinear effects.

The stability boundary is obtained by conducting a similar analysis at different free-stream Mach numbers. Figure 3 shows the buffet-onset boundary for the NACA0012 airfoil. The solid line is the prediction from global-stability theory (with  $N_{SC} = 80$ ) and the open circles are from the experiment of McDevitt & Okuno (1985). Also plotted are results from URANS calculations, where the solid symbols show conditions that remain steady and the open symbols show conditions that are unsteady. The theory, experiment, and URANS calculations are all in very good agreement for  $M < 0.8$ . This good agreement provides evidence for global instability being the cause for transonic-airfoil buffet onset.

Around  $M = 0.8$  the experiment shows an earlier onset of unsteadiness compared to the theory and computations. The stability theory shows significantly smaller growth rates associated with the instability at  $M = 0.8$  as compared to  $M = 0.76$ . At Mach numbers beyond  $M \approx 0.8$ , the flow is stable. The URANS provides on steady solutions for  $M \geq 0.8$ ; this is consistent with the stability results showing small growth rates at  $M = 0.8$ , which can be damped by numerical dissipation in the time evolution of the URANS. An effort to identify additional unstable modes at lower  $\alpha$  showed nothing that could explain the difference with the experiment. Since the URANS and the stability theory are in general agreement regarding the initial onset of unsteadiness, the discrepancy with the experiment is likely the results of deficiencies in the calculated steady flow affecting both the stability and the URANS (e.g. from turbulence modeling) or deficiencies in the experiment.

We now examine characteristics of the separated flow at and around the buffet-onset condition. Figure 4 shows the steady-state skin-friction coefficient downstream of the shock for three different free-stream Mach numbers. In each case, the solid line corresponds to an angle of attack just below the predicted

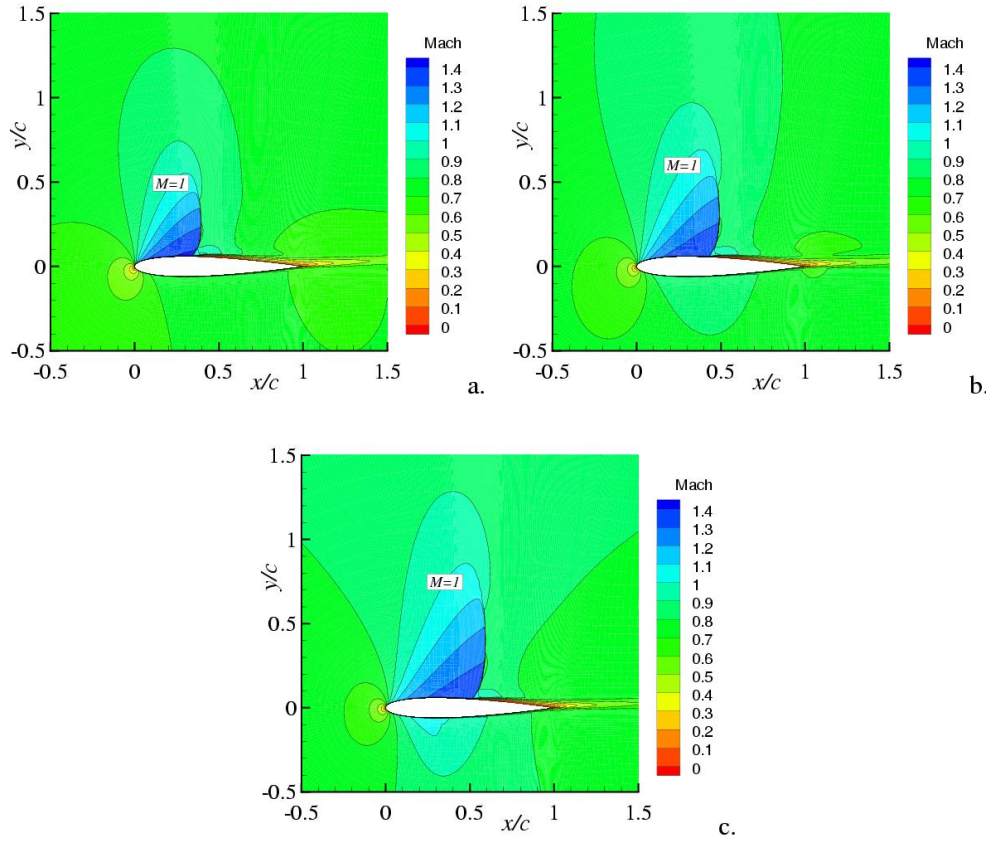


FIGURE 1. Mach contours from RANS calculations at angles of attack just below buffet onset. NACA0012 airfoil results at the conditions: a. ( $M = 0.72$ ,  $\alpha = 4.1^\circ$ ), b. ( $M = 0.76$ ,  $\alpha = 3.0^\circ$ ), c. ( $M = 0.80$ ,  $\alpha = 1.9^\circ$ ), and  $Re = 10^7$ .

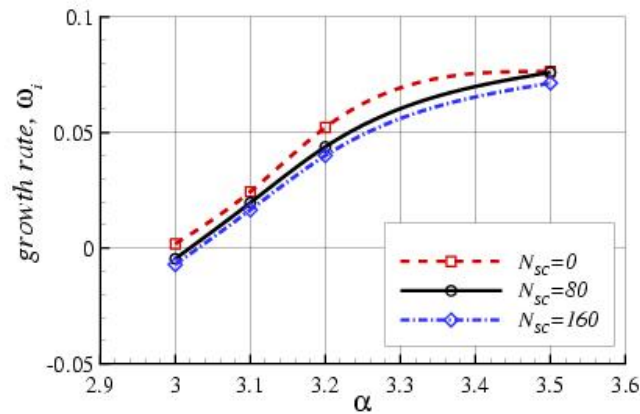


FIGURE 2. Variation of growth rate with airfoil angle of attack for different levels of smoothing, ( $N_{SC} = 0, 80, 160$ ), at  $M = 0.76$ ,  $Re = 10^7$ .

buffet onset, and the dashed line is for an angle of attack just above the predicted buffet onset – thus, bounding the onset condition. For  $M = 0.76$  (Figure 4b), the pre-buffet flow exhibits a separation bubble starting at the foot of the shock, which is near to “bursting.” This behavior is roughly in agreement with the idea that buffet onset occurs once the separation bubble extends from the shock to the trailing edge (Pearcey 1958; Pearcey & Holder 1962). However, for  $M = 0.72$  (Figure 4a) the steady flow exhibits a bubble both before and after the predicted buffet onset condition – showing no link between bubble

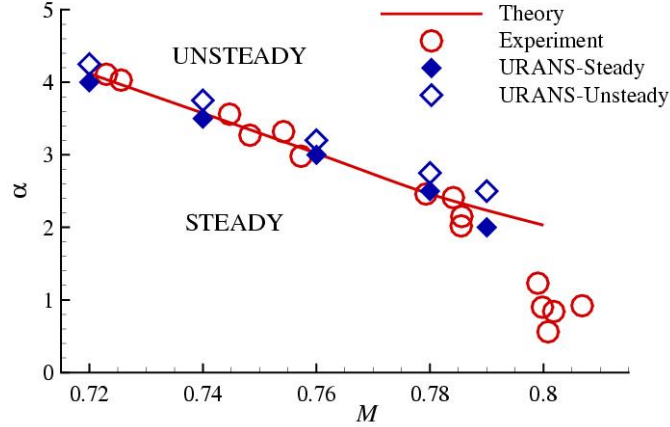


FIGURE 3. Buffet-onset boundary with URANS simulation results and experimental data of McDevitt & Okuno (1985), ( $Re = 10^7$ ).

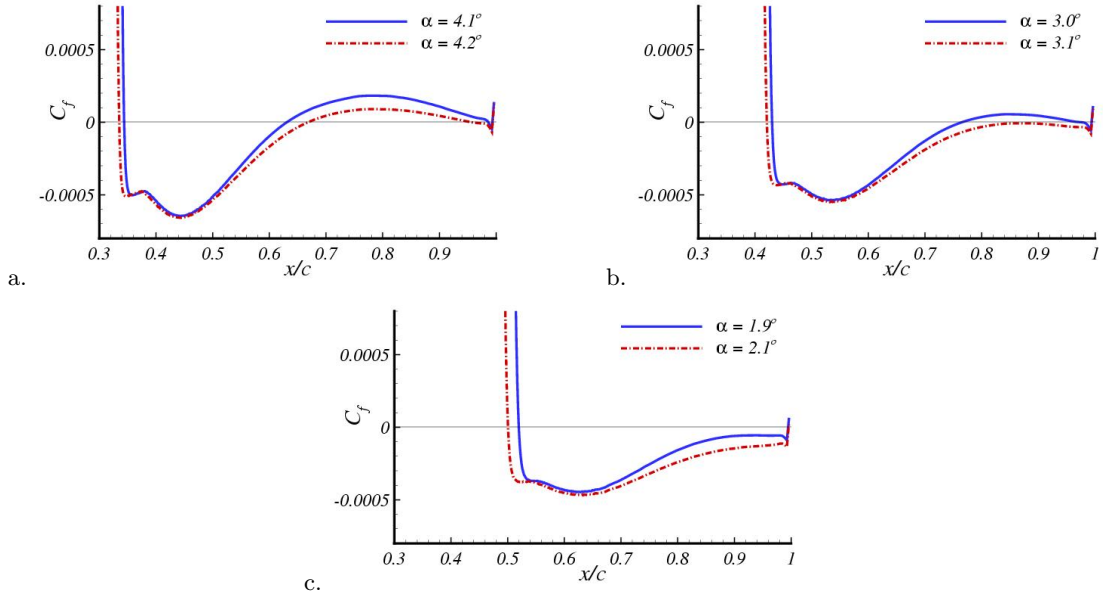


FIGURE 4. Skin friction coefficient from RANS calculations at angles of attack just below (solid line) and above (dashed line) the predicted buffet onset. NACA0012 airfoil results at the conditions: a. ( $M = 0.72$ ), b. ( $M = 0.76$ ), c. ( $M = 0.80$ ), and  $Re = 10^7$ .

“bursting” and buffet onset. Meanwhile, for  $M = 0.8$  (Figure 4c) the flow is separated from the foot of the shock both before and after the predicted buffet-onset condition. The experiments show buffet onset at  $\alpha \approx 1^\circ$  for  $M = 0.80$  (see Figure 3). The steady RANS solution shows attached flow at the trailing edge for  $\alpha \approx 1^\circ$ . Overall, the results for the NACA0012 airfoil do not show a clear link between buffet onset and the qualitative features of the flow separation.

#### 4. Buffeting flow

At buffet onset, the shock begins to oscillate fore and aft (McDevitt & Okuno 1985; Lee 1990; Bartels & Edwards 1997; Jacquin *et al.* 2005). Meanwhile, the boundary layer downstream of the shock exhibits a periodic thickening and thinning, which is phase locked to the shock motion. The velocity component of the global instability ( $u'$  in eqn. (5)) exhibits this exact behavior – although its applicability is limited to small amplitudes. Figure 5 shows six snapshots of the corresponding unsteady pressure for the unstable flow at  $M = 0.76$ ,  $\alpha = 3.2$ . The pressure fluctuation appears to originate near the base of the shock. The

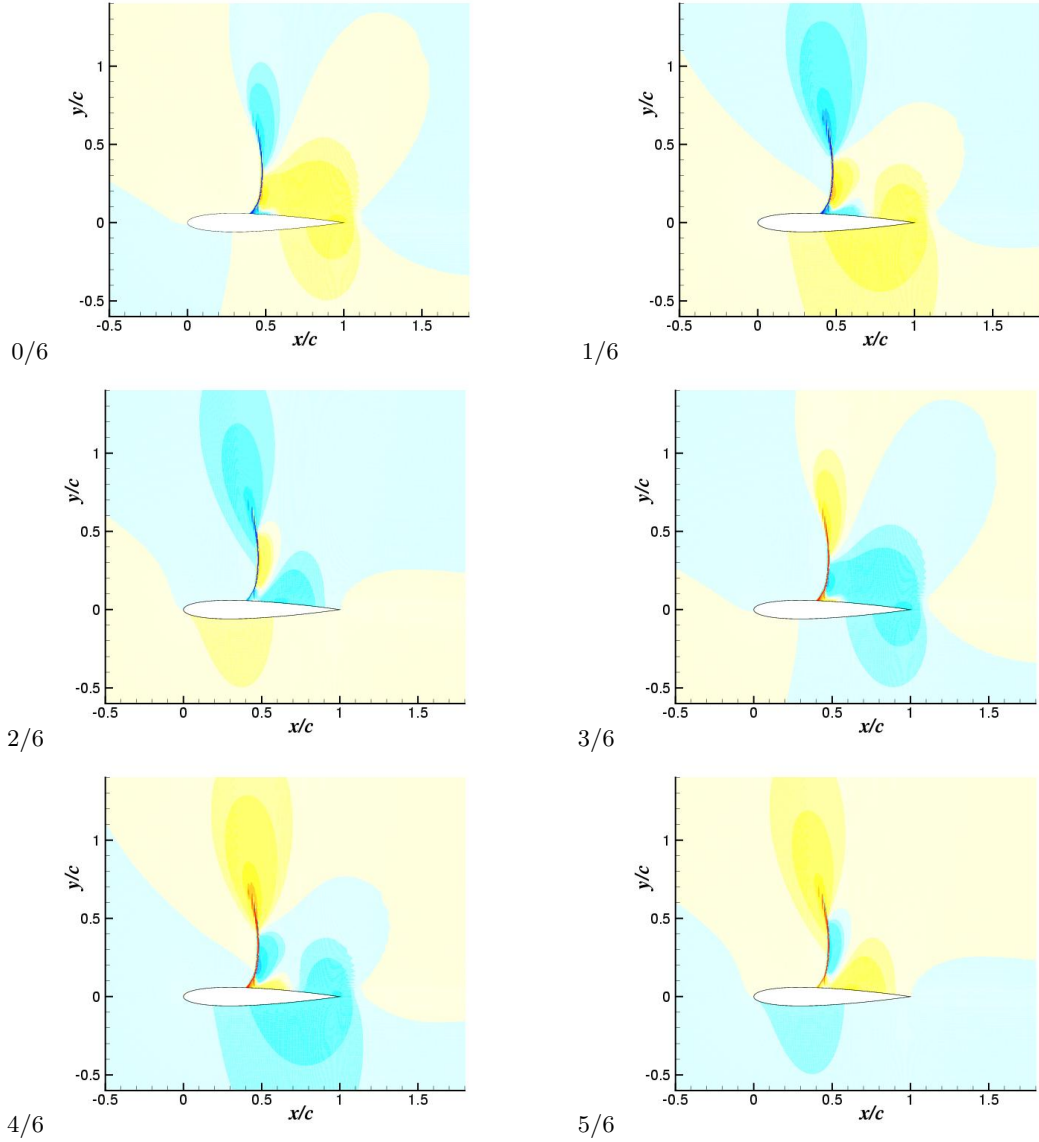


FIGURE 5. Countours of the pressure fluctuation at six steps during the oscillation cycle,  $t/T = 0, 1/6, 2/6, 3/6, 4/6, 5/6$ , for the conditions  $M = 0.76$ ,  $\alpha = 3.2^\circ$ ,  $Re = 10^7$ .

pressure perturbation moves upward along the shock until reaching the top of the sonic zone. It then moves forward becoming ingested into the zone of sonic flow. As the pressure perturbation moves upward along the shock, it also moves aft – intensifying as it approaches the trailing edge. The pressure wave goes around the trailing edge and then propagates forward along the lower surface. The pressure fluctuation is relatively weak at the leading edge where it experiences a significant phase shift before being ingested into the sonic zone. This unsteady flow structure is also seen in the URANS for  $M = 0.76$ ,  $\alpha = 3.25^\circ$ , where the peak-to-peak shock motion is  $\Delta x_{shock}/c \approx 0.1$  (see figure 6). This behavior is qualitatively different from the working model proposed by Lee (1990). In that model, buffet was assumed to result from a feedback cycle between the shock and the trailing edge. Pressure waves generated at the shock propagate downstream inside the boundary layer and are scattered at the trailing edge, resulting in upstream-propagating waves outside the boundary layer; when these wave impact the shock they generate new waves starting a new cycle.

Figure 6 shows the variation of the peak-to-peak amplitude of the shock oscillation  $\Delta x_{shock}/c$  and the surface pressure fluctuation  $p'/p_0$  at  $x/c = 0.8$  as obtained from the URANS. Assuming zero amplitude at  $\alpha \approx 3.02^\circ$ , both of these measures of the disturbance amplitude initially increase rapidly with  $\alpha$ .

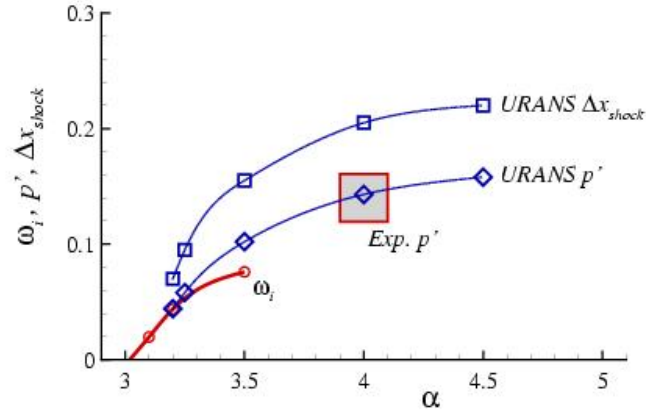


FIGURE 6. Variation of URANS peak-to-peak amplitudes  $\Delta x_{shock}$  and  $p'/p_0$  with airfoil angle of attack for  $M = 0.76$ ,  $Re = 10^7$ . Also shown is the instability growth rate and the  $p'/p_0$  observed in the experiments of McDevitt & Okuno (1985).

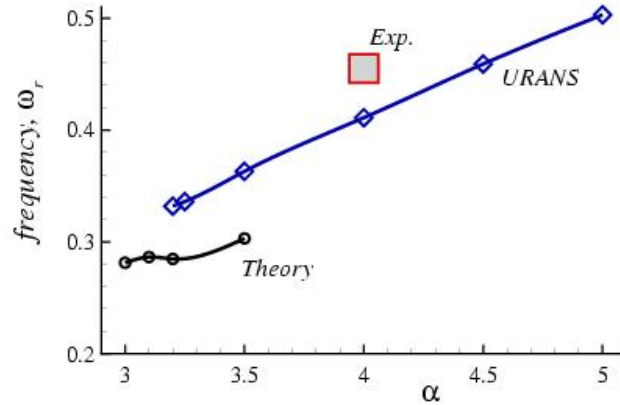


FIGURE 7. Variation of frequency with airfoil angle of attack for  $M = 0.76$ ,  $Re = 10^7$ . The experimental value is from McDevitt & Okuno (1985).

It is not possible to get unsteady solutions with URANS below  $\alpha \approx 3.2^\circ$  because the relatively-weak unsteadiness (very-small growth rate) appears to be damped by numerical dissipation. At higher angles of attack the fluctuation amplitude appears to saturate. This behavior is in general agreement with the experiment of McDevitt & Okuno (1985), which shows rapidly increasing  $p'$  amplitude with  $\alpha$ , followed by an amplitude saturation. The large square on Figure 6 shows an estimate for the  $p'$  amplitude taken from the experiment at a slightly higher Mach number,  $M \approx 0.77$ . Near buffet onset, the instability growth rate also exhibits near-linear variation with the angle of attack. Thus, the amplitude variation near the critical conditions is consistent with a supercritical bifurcation from a weakly-nonlinear theory (Drazin & Reid 1981).

Figure 7 shows the variation of the buffeting frequency as the angle of attack increases. Near buffet onset  $\alpha \approx 3.2^\circ$ , the URANS is within 15% of the global-stability result. As  $\alpha$  is increased, the stability theory shows a weak variation in frequency with  $\alpha$ . By contrast, the URANS frequency rises by 50% over  $1.5^\circ$  of  $\alpha$  variation. The large symbol shows an estimate for the experimental frequency for these conditions – in general agreement with the URANS. The significant rise in the URANS frequency while the instability frequency is nearly constant is similar to the frequency variation for the early vortex shedding on a circular cylinder with increasing Reynolds number (Crouch, Garbaruk & Magidov 2007).

## 5. Conclusions

Buffet onset is analyzed following the global-stability formulation of Crouch, Garbaruk & Magidov (2007), and the URANS numerical-simulation approach as implemented in the NTS code (Strelets 2001). The analysis shows the origin of buffet onset is tied to a global instability. The buffeting flow in the neighborhood of the onset condition is consistent with a supercritical Hopf bifurcation. Global-stability analysis provides a good qualitative and quantitative descriptor for buffet onset. The method provides better predictive capability than earlier empirical and heuristic models, which are currently in use.

## REFERENCES

- McDevitt, J.B. and Okuno, A.F. "Static and dynamic pressure measurements on a NACA0012 airfoil in the Ames high Reynolds number facility," NASA Tech. Paper No. 2485, 1985.
- Bartels, R.E. and Edwards, J.W. "Cryogenic tunnel pressure measurements on a supercritical airfoil for several shock buffet conditions," NASA Tech. Mem. 110272, 1997.
- Jacquin, L., Molton, P., Deck, S., Maury, B. and Soulevant, D. "An experimental study of shock oscillation over a transonic supercritical profile," AIAA Paper No. 2005-4902, 2005.
- Lee, B.H.K. "Oscillatory shock motion caused by transonic shock boundary-layer interaction," *AIAA J.*, Vol. 28, pp. 942-944, 1990.
- Lee, B.H.K. "Self-sustained shock oscillation on airfoils at transonic speeds," *Prog. Aero. Sci.*, Vol. 37, pp. 147-196, 2001.
- Mabey, D.G., Welsh, B.L. and Cripps, B.E. "Periodic flows on a rigid 14% thick biconvex wing at transonic speeds," TR 81059, Royal Aircraft Establishment, 1981.
- Pearcey, H.H. "A method for the prediction of the onset of buffeting and other separation effects from wind tunnel tests on rigid models," AGARD Report 223, 1958.
- Pearcey, H.H. and Holder, D.W. "Simple methods for the prediction of wing buffeting resulting from bubble type separation," NPL AERO-REP-1024, National Physical Laboratory, 1962.
- Drazin, P.G. and Reid, W.H. *Hydrodynamic Stability*, Cambridge University Press, 1981.
- Theofilis, V. "Advances in global linear instability analysis of nonparallel and three-dimensional flows," *Prog. Aero. Sci.*, **39**, pp. 249-315, 2003.
- Crouch, J.D., Garbaruk, A. and Magidov, D. "Predicting the onset of flow unsteadiness based on global instability," *J. Comp. Phys.*, Vol. 224, pp. 924-940, 2007.
- Crouch, J.D., Garbaruk, A., Magidov, D. and Jacquin, L. "Global structure of buffeting flow on transonic airfoils," Proc. IUTAM Symposium on Unsteady Separated Flows and Their Control, to appear.
- Spalart P.R., Allmaras, S.R. "A one-equation turbulence model for aerodynamic flows," *La Recherche Aéronautique*, No. 1, pp. 5-21, 1994, also AIAA Paper No. 92-0439.
- Spalart P.R. "Trends in Turbulence Treatments," AIAA Paper No. 2000-2306, 2000.
- Roe P.L. "Approximate Riemann solvers, parameters vectors and difference schemes," *J. Comp. Phys.*, Vol. 43, pp. 357-372, 1981.
- Lehoucq, R.B., Sorensen, D.C. and Yang, C. *ARPACK user's guide*, SIAM publication, 1998.
- Strelets, M., "Detached-eddy simulation of massively separated flows," AIAA Paper No. 2001-0879, 2001.